

# Spatiotemporal pattern formation in a prey-predator model under environmental driving forces

**Anuj Kumar Sirohi**

School of Computational and Integrative Sciences, Jawaharlal Nehru University, New Delhi-110067, INDIA

E-mail: [anujsirohi.amu@gmail.com](mailto:anujsirohi.amu@gmail.com)

**Malay Banerjee**

Department of Mathematics and Statistics, Indian Institute of Technology, Kanpur-208016, INDIA

E-mail: [malayb@iitk.ac.in](mailto:malayb@iitk.ac.in)

**Anirban Chakraborti**

School of Computational and Integrative Sciences, Jawaharlal Nehru University, New Delhi-110067, INDIA

E-mail: [anirban@jnu.ac.in](mailto:anirban@jnu.ac.in)

**Abstract.** Many existing studies on pattern formation in the reaction-diffusion systems rely on deterministic models. However, environmental noise is often a major factor which leads to significant changes in the spatiotemporal dynamics. In this paper, we focus on the spatiotemporal patterns produced by the predator-prey model with ratio-dependent functional response and density dependent death rate of predator. We get the reaction-diffusion equations incorporating the self-diffusion terms, corresponding to random movement of the individuals within two dimensional habitats, into the growth equations for the prey and predator population. In order to have the noise added model, small amplitude heterogeneous perturbations to the linear intrinsic growth rates are introduced using uncorrelated Gaussian white noise terms. For the noise added system, we then observe spatial patterns for the parameter values lying outside the Turing instability region. With thorough numerical simulations we characterize the patterns corresponding to Turing and Turing-Hopf domain and study their dependence on different system parameters like noise-intensity, etc.

## 1. Introduction

Self-organizing spatial pattern formation in interacting population models is an important area of research to understand the distribution of the species within their habitats. Mainly reaction-diffusion equation models are studied analytically with supportive numerical simulations to understand the nature of population patches and whether they are changing with respect to time or not. Investigations for various types of Turing and non-Turing pattern formations in two dimensional prey-predator models have received significant attention [1, 2, 3, 4, 5]. Spatiotemporal prey-predator models exhibit various types of self-organizing spatial patterns; either

they are stationary or non-stationary. Stationary patterns are characterized by heterogeneous distribution of populations over space which do not change with time once they reach the non-constant steady-state. On the other hand, the non-stationary patterns change with time continuously and never reach any non-constant steady-state. The stationary patterns produced by the spatio-temporal prey-predator models for two dimensional spatial domains can be classified as: (i) spot patterns (cold-spots and hot-spots), (ii) labyrinthine/stripe patterns, or (iii) the mixture of spot and stripe patterns. These three types of patterns are mostly observed for parameter values taken from Turing-domain or Turing-Hopf-domain, when the diffusivity of two species differ by a significant magnitude. Sometimes one does find labyrinthine patterns as a non-stationary pattern but for parameter values well inside the Turing-Hopf domain. The non-stationary patterns may include periodic patterns (sometimes as periodic traveling waves), interacting spiral patterns and chaotic patterns. The occurrences of spatio-temporal chaos for parameter values lying within the Turing domain or outside the Turing-domain remains a debatable and controversial issue [6]. There is no unified approach in determining the parameter values in a systematic way or in identifying the mechanism which leads to the spatio-temporal chaotic patterns [2, 7]. Derivation of necessary-sufficient condition(s), either in terms of parametric restrictions or system characterization for the onset of spatio-temporal chaotic patterns for prey-predator type interacting models thus remains an open problem.

Recently, the role of environmental noise on spatio-temporal pattern formation has been studied by the researchers for the noise added spatio-temporal models of interacting populations [8, 9, 10, 11]. In most of the cases, the authors have been used temporally correlated and spatially uncorrelated coloured noise terms. Although in some investigations the alteration of spatial patterns due to the presence of additive coloured noise terms have been reported but this type of formulation is not ecologically viable as they correspond to spontaneous generation or inhibition of populations at the places with no population or very low concentration of population. On contrary, the consideration of multiplicative noise terms signify the noisy variation in some system parameters involved with the reaction kinetics. It is evident that due to the environmental fluctuations, the carrying capacity, birth and death rates, intensity of intra- and inter-species competition rates, predation rates exhibit random fluctuations to a modular extent around some average value [12]. Perturbation of one or more rate constants by the noise terms leads to spatio-temporal models with multiplicative noise terms. Several noise induced phenomena like noise-induced phase transitions, noise enhanced stability/instability, noise delayed extinction, stochastic resonance are investigated for the spatio-temporal ecological models considered within fluctuating environments. These analytical/numerical findings provide important information towards how the species establish within their respective habitats or help us to identify the important risk factors leading towards the extinction of species.

The main objective of this paper is to study a simple model of predator-prey with ratio-dependent functional response and density dependent death rate of predator, along with the self-diffusion terms corresponding to the random movement of the individuals within two dimensional habitats, and study the influence of small amplitude heterogeneous perturbations to the linear intrinsic growth rates.

## 2. The spatiotemporal model

Consider that  $u \equiv u(x, y, t)$  and  $v \equiv v(x, y, t)$  represent the prey and predator population densities at any time  $t$  and at the spatial location  $(x, y) \in \Omega$ , where  $\Omega \in \mathbb{R}^2$  is a square domain in  $\mathbb{R}$  with boundary  $\partial\Omega$ . The spatiotemporal dynamics of prey-predator interaction with logistic growth for prey, ratio-dependent functional response and density dependent death rate for predators is governed by the following system of nonlinear coupled partial differential equations (PDE), in terms of dimensionless variables and parameters:

$$\frac{\partial u}{\partial t} = u(1-u) - \frac{\alpha uv}{u+v} + \nabla^2 u \equiv f(u, v) + \nabla^2 u, \quad (1)$$

$$\frac{\partial v}{\partial t} = \frac{\beta uv}{u+v} - \gamma v - \delta v^2 + d\nabla^2 v \equiv g(u, v) + \nabla^2 v \quad (2)$$

subjected to positive initial conditions:

$$u(x, y, 0) \equiv u_0(x, y) > 0, v(x, y, 0) \equiv v_0(x, y) > 0, \text{ for all } (x, y) \in \Omega \quad (3)$$

and zero-flux boundary conditions:

$$\frac{\partial u}{\partial \nu} = \frac{\partial v}{\partial \nu} = 0, \text{ for all } (x, y) \in \partial\Omega, t > 0 \quad (4)$$

where  $\nu$  is the outward drawn unit normal vector on the boundary, and  $\alpha, \beta, \gamma$  and  $\delta$  are positive dimensionless parameters. The ratio of diffusivity of two species is denoted as  $d$ . The diffusion terms in this reaction-diffusion system for the prey and predator population are introduced to take care of the random movements of the individuals within two dimensional habitats. The zero-flux boundary condition indicates that predator-prey system is self-contained within the two dimensional habitat with no population flux across the boundary.

### 2.1. Turing Bifurcation

The ecologically feasible and coexisting equilibrium point for the corresponding temporal model are spatially homogeneous steady state for the reaction diffusion model (1-2) and can be obtained by solving the following two algebraic equations, with  $u, v > 0$ :

$$f(u, v) = u(1-u) - \frac{\alpha uv}{u+v} = 0, \quad (5)$$

$$g(u, v) = \frac{\beta uv}{u+v} - \gamma v - \delta v^2 = 0. \quad (6)$$

If we denote the coexisting equilibrium point by  $E_*(u_*, v_*)$ , then  $u_*$  and  $v_*$  satisfy the equations  $1 - u - \frac{\alpha v}{u+v} = 0 = \frac{\beta u}{u+v} - \gamma - \delta v$ . The explicit expression for the components of  $E_*$ , conditions for their feasible existence and possible number of coexisting steady-states are discussed in Ref. [7] extensively. Further we assume that  $E_*$  is coexisting homogeneous steady-state which is locally asymptotically stable for the temporal counterpart of the system (1-2), i.e., the conditions  $a_{11} + a_{22} < 0$  and  $a_{11}a_{22} - a_{12}a_{21} > 0$  are simultaneously satisfied, where  $a_{11}, a_{12}, a_{21}$  and  $a_{22}$  are given by

$$a_{11} = 1 - 2u_* - \frac{\alpha v_*^2}{(u_* + v_*)^2}, \quad a_{12} = -\frac{\alpha u_*^2}{(u_* + v_*)^2}, \quad a_{21} = \frac{\beta v_*^2}{(u_* + v_*)^2},$$

$$a_{22} = -\gamma - 2\delta v_* + \frac{\beta u_*^2}{(u_* + v_*)^2}.$$

The basic criteria for the diffusion-driven instability or Turing instability is that the stable homogeneous steady-state becomes unstable due to small amplitude heterogeneous perturbation around the homogeneous steady-state. Hence for the occurrence of Turing instability, first we need a locally stable coexisting steady-state for the corresponding temporal model. The linear stability analysis for spatiotemporal model (1-2) around the homogeneous steady-state  $E_*$

and the conditions required for the onset of Turing-instability are well established and used by several researchers. Here, we just mention the three basic mathematical criteria required for Turing-instability of the model (1-2) around  $E_*(u_*, v_*)$ , as follows:

$$a_{11} + a_{22} < 0, \quad (7)$$

$$a_{11}a_{22} - a_{12}a_{21} > 0, \quad (8)$$

$$da_{11} + a_{22} > 2\sqrt{d}\sqrt{a_{11}a_{22} - a_{12}a_{21}}, \quad (9)$$

and Turing-instability sets in at the critical wave number

$$k_{cr}^2 = \frac{da_{11} + a_{22}}{2\sqrt{d}} > 0. \quad (10)$$

Satisfaction of the condition (9) implies homogeneous steady-state becomes unstable under small amplitude heterogeneous perturbation for wavenumbers  $k > k_{cr}$  and Turing pattern emerges. Type(s) of emerging spatial pattern(s) (as mentioned earlier in the introduction), depend upon the specific choice of parametric values and magnitude of  $d$ .

The Turing-bifurcation curve is defined by the following equation

$$da_{11} + a_{22} = 2\sqrt{d}\sqrt{a_{11}a_{22} - a_{12}a_{21}}.$$

Solving this equation for  $d$ , we can find the critical threshold for the ratio of diffusivity  $d_{cr}$ , above which the Turing patterns emerge. In the next section we are going to report the varieties of spatial patterns generated by the system (1-2) for suitable choice of the parameter values satisfying the Turing bifurcation conditions.

### 3. Self-organizing spatial patterns

In this section, we present the numerical simulation results and varieties of spatial patterns that are exhibited by the spatiotemporal model (1-2) for parameter values within the Turing and Turing-Hopf domain. If we take the parameter values  $\alpha = 2.0$ ,  $\beta = 1$ ,  $\gamma = 0.6$  and  $\delta = 0.1$  then we find the unique coexisting equilibrium point  $E_*(0.2287, 0.1436)$  which is a homogeneous steady-state for the system (1-2).  $E_*$  is locally asymptotically stable for the temporal counterpart as the conditions (7) and (8) are satisfied. In order to understand the role of diffusivity of the prey and the predator towards the destabilization of the homogeneous steady-state we need to find the quantity  $d_{cr}$  as mentioned in the previous section. For the chosen set of parameter values, we find  $d_{cr} = 4.9157$  and hence the heterogeneous perturbations lead to Turing patterns for  $d > d_{cr}$ .

The existence and non-existence of Turing patterns are solely dependent upon the magnitude of the parameters involved with the model under consideration. Here we consider  $\alpha$  and  $d$  as the bifurcation parameters to construct the Turing bifurcation diagram. We have presented the Turing bifurcation diagram in  $\alpha d$ -parametric plane (see Fig. 1). The bifurcation diagram is prepared keeping  $\beta = 1$ ,  $\gamma = 0.6$  and  $\delta = 0.1$  fixed.  $\alpha$  and  $d$  are considered as the controlling parameters to obtain different spatiotemporal patterns. We have presented three bifurcation curves in the bifurcation diagram, namely Turing-bifurcation curve (blue curve), temporal Hopf-bifurcation curve (red dashed line) and temporal homoclinic bifurcation curve (black dotted curve). The coexisting equilibrium point  $E_*$  for the temporal model, corresponding to the system (1-2), is stable for  $\alpha < \alpha_h$  and it loses stability through the Hopf-bifurcation at  $\alpha_h = 2.01$  (approx). The Turing instability region is the region lying above the Turing bifurcation curve and which is divided into two parts by the vertical line  $\alpha = \alpha_h$ . Part of

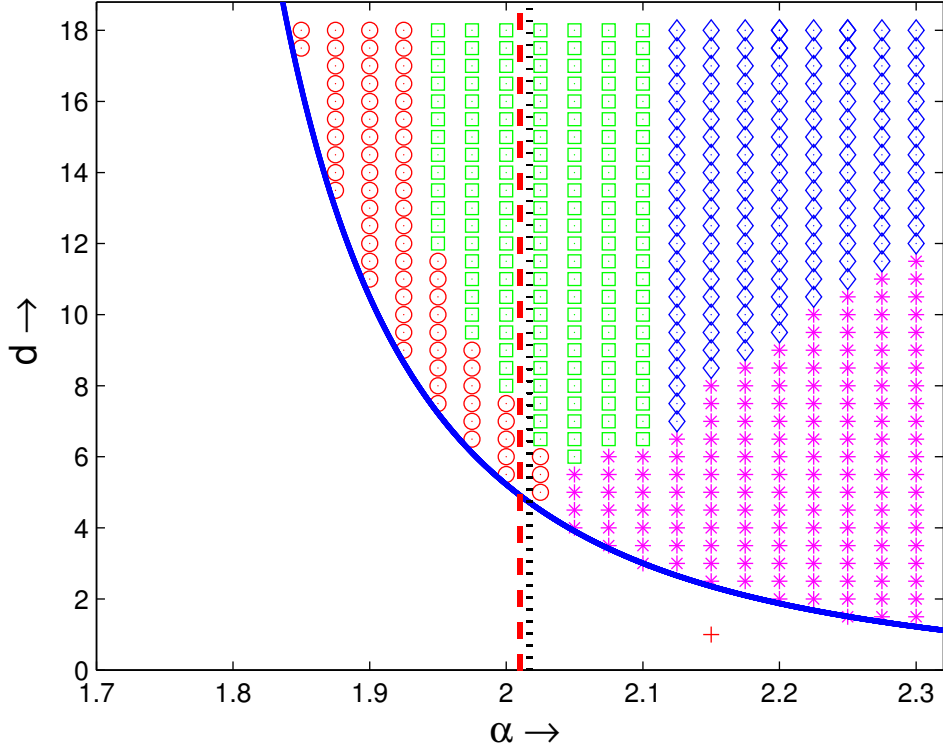


**Figure 1.** Five different types of spatial patterns observed for the parameter values lying within the Turing instability region (above the blue curve which is Turing bifurcation curve) and below Turing instability region. Choices of parameter values are marked with four different symbols based upon the resulting patterns:  $\circ$  cold-spot,  $\square$  mixture of spot-stripe,  $\diamond$  labyrinthine,  $*$  chaotic and  $+$  interacting spiral. Hopf-bifurcation curve (shown by red dashed line) and temporal homoclinic bifurcation curve (shown by black dotted curve).

the Turing domain lying in the region  $\alpha > \alpha_h$  is the Turing-Hopf domain where temporal and spatiotemporal perturbations are both unstable.

For the chosen set of parameter values we find only one feasible coexisting equilibrium point  $E_*$  therefore we will discuss only the spatial-pattern formation around this homogeneous steady-state. We have obtained various patterns generated by the model under consideration through exhaustive numerical simulations. All numerical simulations are carried out over a  $200 \times 200$  lattice with time-step  $\Delta t = 0.01$  and spatial steps  $\Delta x = \Delta y = 2$ . All numerical simulations are performed using the forward Euler method for the temporal part and five point finite difference scheme for the diffusion part. A small amplitude heterogeneous perturbations to the homogeneous steady-state are introduced by  $u_0(x_i, y_j) = u_* + \epsilon \xi_{ij}$ ,  $v_0(x_i, y_j) = v_* + \epsilon \eta_{ij}$  where  $\epsilon = 0.001$ ,  $\xi_{ij}$  and  $\eta_{ij}$  ( $i, j = 1, 2$ ) are spatially uncorrelated Gaussian white noise terms. We have observed four different types of patterns within the Turing domain, cold-spot, labyrinthine, mixture of spot and stripe and spatiotemporal chaotic patterns.

We have observed only cold-spot and mixture of spot-stripe patterns for parameter values within the Turing domain, whereas mixture of spot-stripe, labyrinthine and chaotic patterns are observed for parameters lying in the Turing-Hopf domain. Numerical simulations have been performed for systematic choices of  $\alpha$  and  $d$  within the Turing domain in order to understand the entire variety of spatiotemporal patterns for parameter values within the Turing domain. Obtained patterns for different combinations of  $\alpha$  and  $d$  are marked with four different symbols.

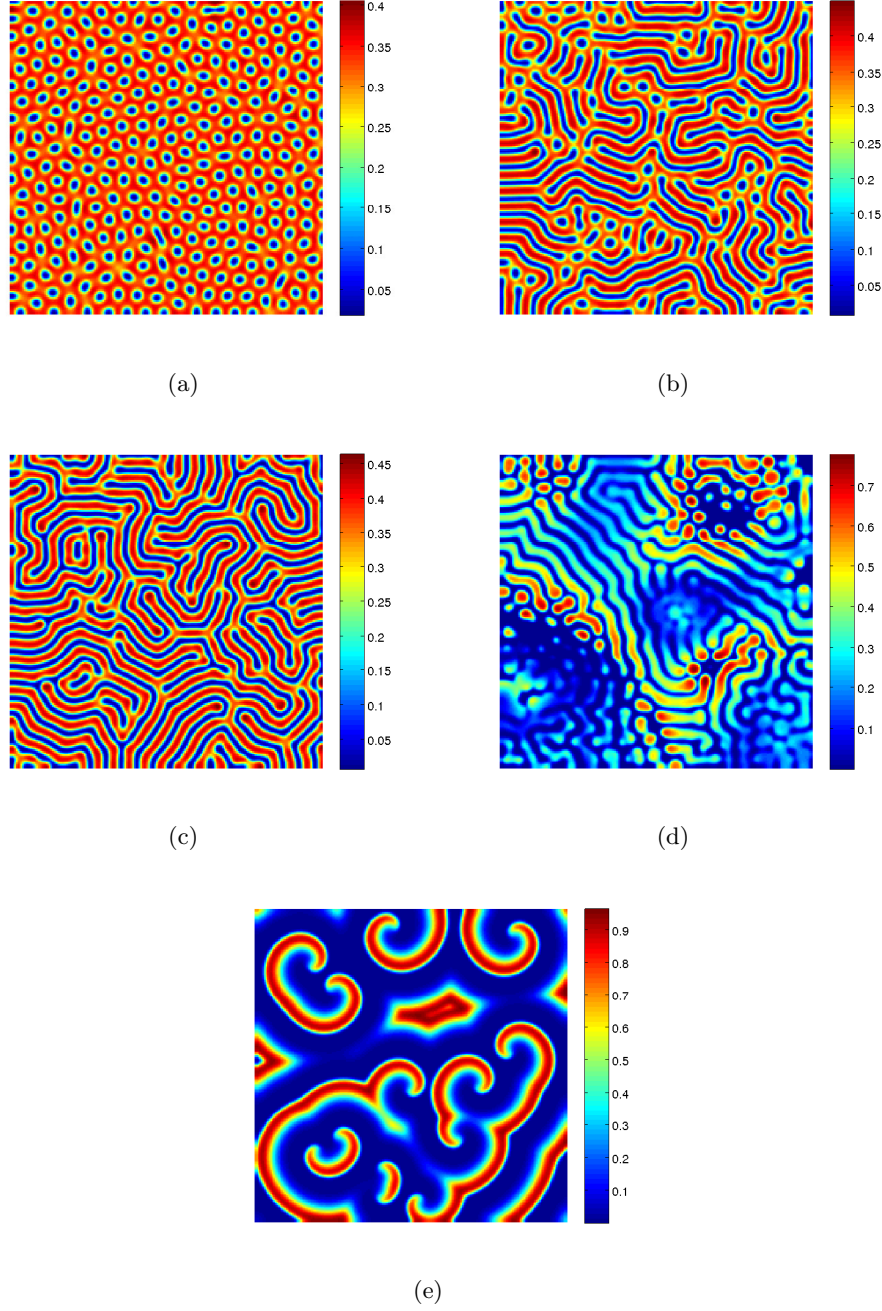


**Figure 2.** Spatial distribution of prey ( $u$ ) obtained at  $t = 1000$  for  $\beta = 1$ ,  $\gamma = 0.6$ ,  $\delta = 0.1$ ,  $d = 10.0$  and (a)  $\alpha = 1.95$ ; (b)  $\alpha = 2.05$ ; (c)  $\alpha = 2.15$ ; (d)  $\alpha = 2.30$ ; and (e)  $d = 1.0$ ,  $\alpha = 2.15$ . The color bar in each panel represents the magnitude of  $u$ .

The whole regime of patterns in the Turing domain is shown in the Fig. 1.

A sample of each type of patterns observed within the Turing domain are shown in Fig. 2. At the lower panel we have presented the interacting spiral pattern which is observed for parameter values just outside the Turing-Hopf domain and for  $d = 1.0$ . As the Turing instability can not occur for  $d = 1.0$ , we can label this pattern as non-Turing pattern. To understand the stationary nature of the observed patterns, we have calculated the time evolution of spatial average for the

prey and predator densities against time corresponding to the patterns reported in Fig. 2 and the results are presented in Fig. 3. The time evolution of  $\langle u \rangle$  and  $\langle v \rangle$  are considered over a longer period of time to ensure that the final observations are far away from the transient behavior. Looking at the time evolution of spatial averages presented at Fig. 3, one can easily understand that cold-spot, mixture of spot-stripe and labyrinthine patterns are stationary patterns whereas the interacting spiral pattern is a non-stationary pattern. The time evolution of the spatial averages are continuously oscillating and never settle down to any stationary value. Corresponding to the spatiotemporal chaotic pattern presented in Fig. 2(d), the time evolution of spatial averages exhibit irregular oscillations for  $t > 650$  and the irregularity sustains at all future time. Here we have presented the results up to  $t = 1000$  from the sake of brevity.

#### 4. Noise Added Model

In this section we are interested to study the effect of noise on the spatiotemporal pattern formation for the model (1-2). For this purpose we introduce uncorrelated multiplicative white noise terms to the growth equations of both the prey and the predator populations, accordingly the noise added model is given by:

$$\frac{\partial u}{\partial t} = u(1 - u) - \frac{\alpha uv}{u+v} + \nabla^2 u + \sigma_1 u \xi_1(t, x, y), \quad (11)$$

$$\frac{\partial v}{\partial t} = \frac{\beta uv}{u+v} - \gamma v - \delta v^2 + \nabla^2 v + \sigma_2 v \xi_2(t, x, y), \quad (12)$$

where  $\xi_1(t, x, y)$  and  $\xi_2(t, x, y)$  are two temporally as well as spatially uncorrelated Gaussian white noise terms. The averages and correlations of the noise functions are given by,

$$\langle \xi_1(t, x, y) \rangle = \langle \xi_2(t, x, y) \rangle = 0$$

$$\langle \xi_j(t, x, y) \xi_j(t_1, x_1, y_1) \rangle = 2\sigma_j \delta(t - t_1) \delta(x - x_1) \delta(y - y_1), j = 1, 2,$$

where  $\sigma_1$  and  $\sigma_2$  are the intensities of the environmental driving forces. The introduction of the noise terms can be justified from ecological point of view also. Here we are considering the dimensionless model and hence we can see from (1-2) that the intrinsic growth rate of the prey is '1' and the intrinsic death rate for the predators is ' $\gamma$ '. Now we assume that the intrinsic growth rate of the prey and the death rate of the predator population are subjected to environmental fluctuations and hence we can perturb them by spatiotemporal noise terms. As a result, if we consider the introduction of noise terms into the said rate constants, that is,  $1 \rightarrow 1 + \sigma_1 \xi_1(t, x, y)$  and  $\gamma \rightarrow \gamma + \sigma_2 \xi_2(t, x, y)$  then we find the noise added model (11) - (12) from the original spatiotemporal model (1-2).

In order to understand the effect of noise on the spatiotemporal pattern formation, we have performed numerical simulations with the changing magnitude of noise intensities. Here we consider the parameter set  $\alpha = 2.15$ ,  $\beta = 1$ ,  $\gamma = 0.6$ ,  $\delta = 0.1$ ,  $d = 8.5$  and assume that both the noise intensities are same, that is  $\sigma_1 = \sigma_2 = \sigma$ . The numerical simulation is performed for  $\sigma = 0.01$  and the resulting distribution of the prey population is shown at Fig. 4(b) along with the pattern observed for  $\sigma = 0$  (see Fig. 4(a)). There is no significant difference in the reported patterns as the noise intensity is small. We have also calculated the spatial averages for the prey and predator populations up to  $t = 3000$  for  $\sigma = 0$  and  $\sigma = 0.0010$  and the results are presented at Fig. 4(c)-(d). It is clear from these figures that the small noise does not change the system characteristics when the spatiotemporal patterns are oscillatory in nature. One can observe similar results for the parameter values corresponding to the stationary patterns and when noise intensities are not very high.

In order to support our claim, we have prepared a bifurcation diagram for the same set of parameter values, as mentioned above, and considering the ratio of diffusivity as the bifurcation

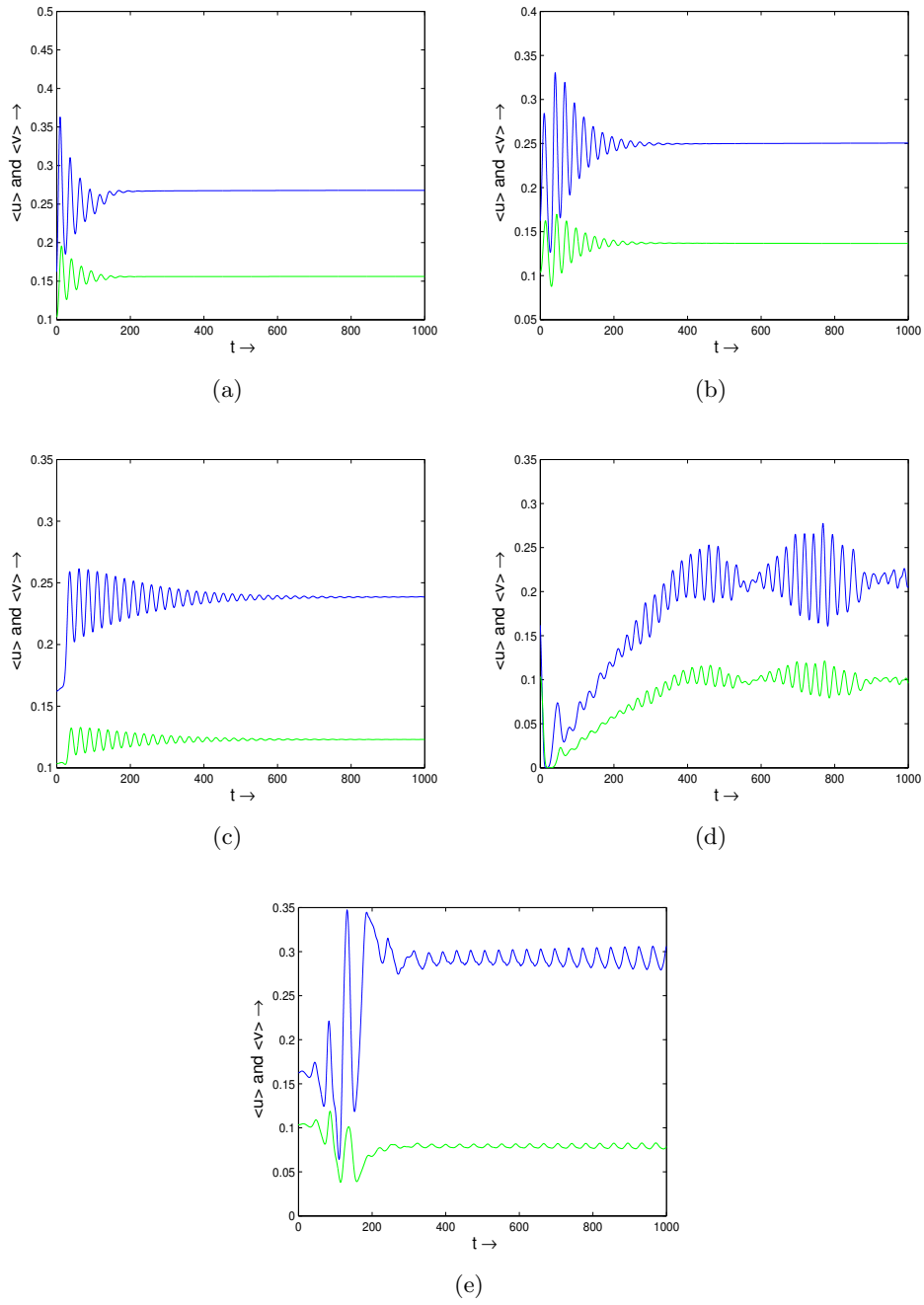


**Figure 3.** Time evolution of spatial averages of the prey  $\langle u \rangle$  and predator  $\langle v \rangle$  populations, presented in (dark) blue and (light) green colors, respectively, for  $t \in [0, 1000]$  corresponding to the patterns presented in Fig. 2.



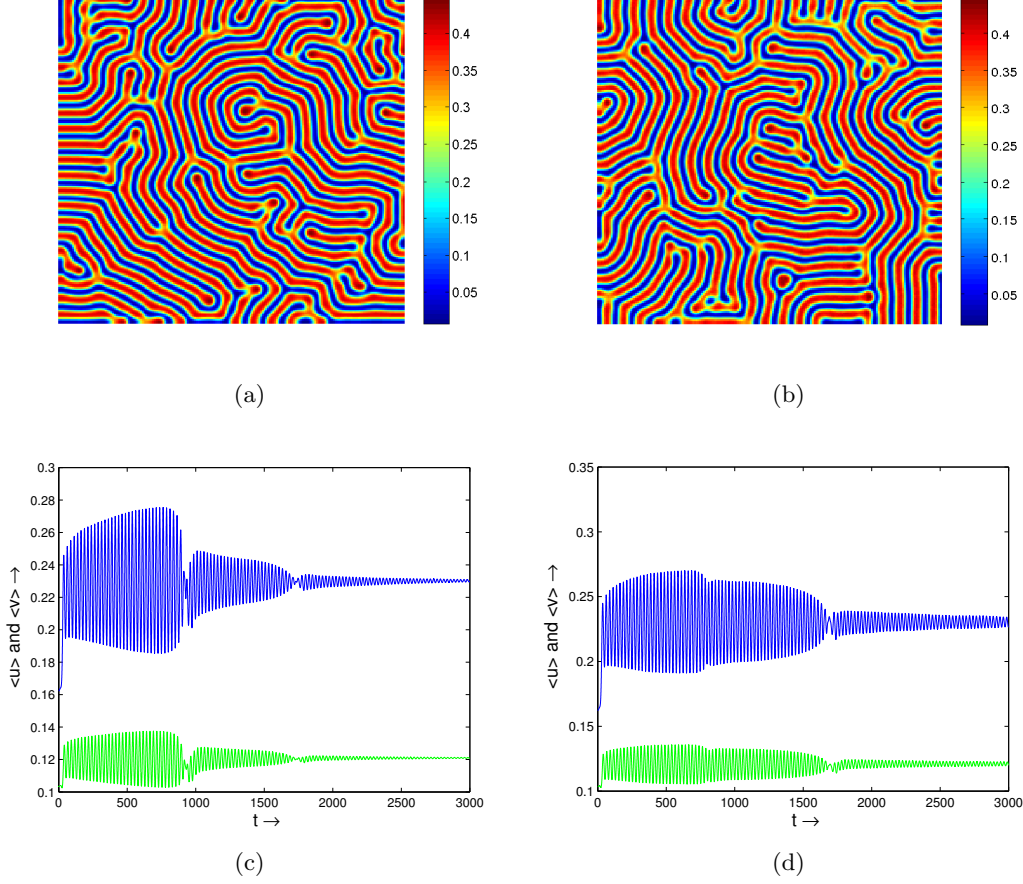


**Figure 4.** Spatial distribution of prey obtained at  $t = 3000$  for  $\alpha = 2.15, \beta = 1, \gamma = 0.6, \delta = 0.1$  and  $d = 8.5$  (a)  $\sigma = 0$  (b)  $\sigma = 0.01$ ; the color bar in each panel represents the magnitude of  $u$ . Time evolution of spatial averages of prey  $\langle u \rangle$  and predator  $\langle v \rangle$  populations in (dark) blue and (light) green colors, respectively, for (c)  $\sigma = 0$ , and (d)  $\sigma = 0.01$ .

parameter. The bifurcation diagrams are prepared for the spatiotemporal model (1-2) as well as for the noise added model (11) - (12) with  $\sigma = 0.01$ , see Fig. 5. We have performed the numerical simulations for  $d = 1.0$  to  $d = 11.0$  with increments of 0.5 and spatial averages are calculated for the prey population up to  $t = 3000$ . After discarding the initial transients, all local maxima and minima of the spatial average of the prey population are plotted against each values of ' $d$ '. If we compare the bifurcation diagrams, then it is evident that the number of local maxima and minima increases with the introduction of small amplitude noise terms mainly within the parameter regime where we find non-stationary spatial patterns in the absence of noise. One natural question arises whether the bifurcation diagram presented at the right panel of Fig. 5 changes from one simulation to other. It does not change as we have taken the spatial average at each time step and the spatial domain is sufficiently large to avoid such kind of variation in the bifurcation diagram.

After understanding the effect of small intensity noise on the resulting patterns, it is important to understand what happens with the increasing magnitude of noise intensities. Of course, we can find some noisy patterns when the magnitude of  $\sigma$  is significantly large and some times it is difficult to identify the particular type of patterns they are representing. In order to avoid this type of confusion and appropriate understanding of the underlying phenomena, we have

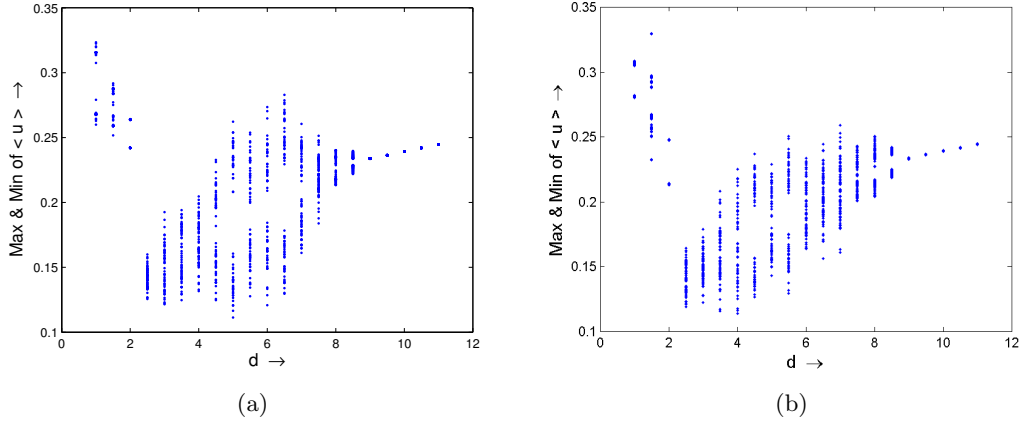


**Figure 5.** Bifurcation diagram with respect to bifurcation parameter  $d$  with other parameters remaining same as in the previous figure for (a)  $\sigma = 0$  and (b)  $\sigma = 0.01$ .

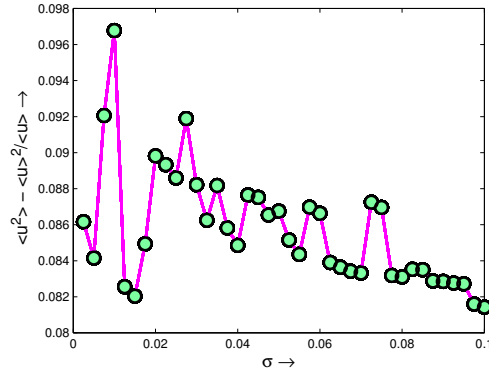


**Figure 6.** Signal to Noise ratio measure for  $\alpha = 2.15$ ,  $\beta = 1$ ,  $\gamma = 0.6$ ,  $\delta = 0.1$ ,  $d = 8.5$ .

calculated the signal-to-noise-ratio (SNR) against a range of noise intensities. Keeping  $\alpha = 2.15$ ,  $\beta = 1$ ,  $\gamma = 0.6$ ,  $\delta = 0.1$ ,  $d = 8.5$  fixed, we have performed the numerical simulations for a range of values of  $\sigma$ . After discarding the initial transients, we have calculated the signal-to-noise-ratio measure  $\frac{\langle u^2 \rangle - \langle u \rangle^2}{\langle u \rangle}$  for  $u(t, x, y)$  obtained at  $t = 3000$  and the average is taken over the entire spatial domain [13]. The plot of the SNR measure is shown at Fig. 6 when  $\sigma$  varies within the range  $[0.0025, 0.1]$ . From the figure, it is evident that the relative variance of the population is not a monotonic increasing function of the noise intensities. The environmental driving force can cause the dispersion of the populations from their average value but the internal mechanism can compensate to maintain the size of the population patches and as a result we find that the relative variance is an increasing function of the noise intensity.

## 5. Conclusion

In this paper, we have studied a predator-prey model with ratio-dependent functional response and density dependent death rate of predator, incorporated with the self-diffusion terms corresponding to the random movement of the individuals within two dimensional habitats. Extensive numerical simulations were performed to understand the regimes of patterns that the model exhibited within and outside of the Turing boundary. Typically, four types of patterns were observed within the Turing domain and interacting spiral pattern as non-Turing pattern.

The effect of environmental driving forces (noise) were also studied. Interestingly, we observed that the small amplitude noise does not alter the stationary pattern; only the time taken to reach the stationary pattern increases. However, irregularity increases even with small noise intensities within the non-stationary regime. We observed that dispersion of population from their spatial average does not increase gradually with the noise intensities; rather noise and demographic interaction play crucial roles to determine the distribution of populations within their habitats, even during the adverse environmental conditions. Our next attempt will be to address the issues of parameter values within the spatiotemporal chaotic domain, and also investigate different noise scenarios such as  $\sigma_1 \neq \sigma_2$ .

## References

- [1] Alonso D, Bartumeus F and Catalan J 2002 *Ecology* **83** 28–34
- [2] Banerjee M and Petrovskii S 2011 *Theoretical Ecology* **4** 37–53
- [3] Baurmann M, Gross T and Feudel U 2007 *Journal of Theoretical Biology* **245** 220–229
- [4] Medvinsky A B, Petrovskii S V, Tikhonova I A, Malchow H and Li B L 2002 *SIAM Review* **44** 311–370
- [5] Wang W, Liu Q X and Jin Z 2007 *Physical Review E* **75** 051913
- [6] Malchow H, Petrovskii S V and Venturino E 2007 *Spatiotemporal Patterns In Ecology And Epidemiology: Theory, Models, And Simulation* (Chapman and Hall/CRC)
- [7] Banerjee M and Banerjee S 2012 *Mathematical Biosciences* **236** 64–76
- [8] Malchow H, Hilker F M, Petrovskii S V and Brauer K 2004 *Ecological Complexity* **1** 211–223
- [9] Sun G Q, Jin Z, Li L and Liu Q X 2009 *Journal of Biological Physics* **35** 185–196
- [10] Wang W, Li W, Li Z and Zhang H 2011 *Biosystems* **104** 48 – 56
- [11] Li L and Jin Z 2012 *Nonlinear Dynamics* **67** 1737–1744
- [12] May R M 1972 *Science* **177** 900–902
- [13] Pikovsky A S and Kurths J 1997 *Physical Review Letters* **78** 775–778